CHAPTER 1

Introduction

1.1 Overview

Nanomaterials are of significant interest in modern science due to their wide range of applications in various disciplines such as sensing, catalysis, data storage, water purification, magnetic resonance imaging, environmental remediation, bioimaging and biomedicine [1-8].

The multifunctional nanoparticles are the nanoparticles or nanoparticle based systems that integrate two or more properties, in which one is normally structural and another one is functional viz. electrical, optical, magnetic etc. [9-11]. Amidst all types of available nanoscale materials, superparamagnetic iron oxide nanoparticles (SPIONs) are the most studied types of nanoparticles for successful use in biomedicine due to their room temperature superparamagnetic properties, intoxicity and low-cost easy synthesis. [12-16]. SPIONs have already been approved by Food and Drug Administration (FDA), USA to be implemented in clinical use for human patients to enhance MRI signals, hyperthermic and targeted drug delivery agents [17-20]. To impart multifunctionality to the synthesized SPIONs, these nanomaterials are coated with optically active metals which make them useful as effective contrast enhancement agent. The iron oxide nanoparticles are functionalized or coated with dyes, surfactants, polymers, silica,

decorated with carbon dots [6, 21–24]. These iron oxides can also be dispersed in a matrix to prevent it from oxidation as well as to make them optically active [22, 25–29]. The functionalization of these nanomaterials makes them exhibit superior optical as well as magnetic properties. There are few disadvantages such as toxicity, photo-bleaching, non-biodegradability, low blood circulation time, complex synthetic procedures and expensive [17, 30-35].

This chapter reviews few most important biological applications of these iron oxide multifunctional nanoparticles, their essential properties and effect of various external and internal parameters on these properties.

1.2 Biological Applications of Multifunctional Nanoparticles

As we have discussed in earlier section, the multifunctional materials exhibit a combination of various properties, these materials have wide biological applications depending upon their suitability. The magnetic nanoparticles, which show plasmonic

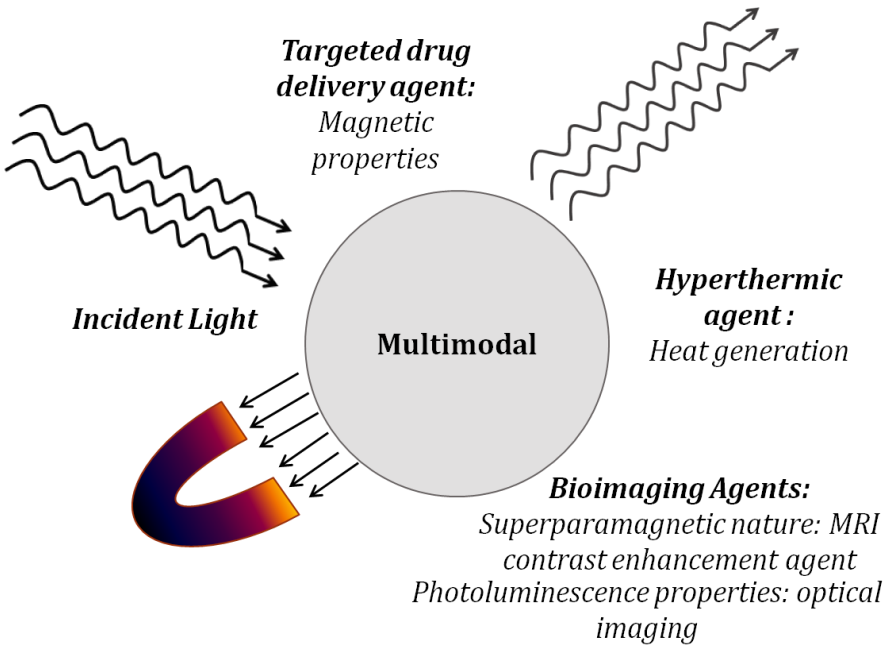

Figure 1.1 Schematic diagram showing various possible applications of a multimodal agent in biomedical field.

activity in the visible region of electromagnetic spectrum, termed as 'magneto-plasmonic' nanostructures have potential applications in biomedical field as shown schematically in Figure 1.1. Even after a decade of research on these materials, their applications are still in innovation stage. It has the capability to be employed as contrast enhancement agent in several imaging modalities, drug delivery and therapeutic agents [30, 36-38]. For the ex-vivo applications, they are best suited material due to their non-toxicity, biocompatibility, colloidal stability and high magnetic moments [39-41]. The most widely used application of these multifunctional SPIONs is as multimodal imaging agents [5, 42-44]. The essential properties of multimodal contrast agents have been discussed in the following section.

1.3 Essential Properties for Multimodal Contrast Agents

The multimodal contrast agents should provide direct and significant visualization of tumors or pathological tissues, long blood circulation time and targeted drug delivery. They should also be biocompatible and useful in therapeutics. The most desirable optical, structural and magnetic characteristics properties are as listed below:

***Luminescence or Surface Plasmon Resonances*:** In order to impart multimodality to the system, a nanoparticle needs to be optically active. The particles with their emission and surface plasmon resonance peak lying in visible region of electromagnetic spectrum are an excellent candidate for multimodal imaging applications [45,46]. The particles with blue or green emission are much preferred over other color emission due to their ability to delineate the abnormal tissues with healthy ones [47]. The materials with photoluminescent properties lying in visible region of spectrum are exploited in development of bioimaging probes [48].

***High Saturation Magnetization*:** The saturation magnetization is unique material property of magnetic materials with a maximum value denoted as M_s. At high enough

values of magnetic field, the magnetization for a material becomes constant at its saturation value of M_s. The nanoparticles with multimodal functionality require high value of saturation magnetization as their relaxation is directly proportional to the square of M_s value [49, 50].

***Superparamagnetism*:** In few materials with particle size below 50 nm where single domains is observed, a specific condition of magnetism termed superparamagnetism comes into the picture [51]. For single-domain particles, in thermodynamic equilibrium in a field, the magnetization behavior is identical to that of paramagnets with exceptionally large susceptibilities for higher magnetic fields. It is one of the most essential properties of the material to be used as multimodal agent [7]. The fundamental theory of superparamagnetism is discussed in detail in the section 1.7.4.

Relaxivity: In magnetic resonance based imaging, the relaxivity is most important parameter. The magnetic nanoparticles are mainly employed as T_2–modulating agents [20, 52-53]. The value of transverse relaxivity R_2 is highly dependent upon crystallinity and saturation magnetization as given by outer sphere spin relaxation approximation: $R_2 = \frac{1}{T_2} = \frac{256\,\pi^2\gamma^2}{405} m_s^2 V \times \frac{r^2}{D\left(1+\frac{L}{r}\right)}$, where γ is the proton's gyromagnetic ratio. The M_s, r and V are saturation magnetization radius and volume fraction of the nanoparticles, respectively; D represents diffusion co-efficient of water molecules and L is the surface coating thickness [54-55]. The higher value of R_2 is desirable for multimodal agents.

***Magnetic Hyperthermia Properties*:** The nanoparticles with size smaller than 100 nm, on application of an external alternating magnetic field, can generate considerable amount of heat which is useful in killing the tumors or cancerous cells inside a human body [56]. The generation of heat occurs via two processes: magnetic spin relaxation through Neel and Brownian relaxation as well as hysteresis losses. The particles with size less than 20 nm contain only single magnetic domain which discards the possibility

of heat generation through hysteresis losses [57]. A rapid increase in temperature or heating of colloidal magnetic fluids which raises the local body temperature in the range 42-45^{0}C on application of an alternating magnetic field (~10-100 mT with frequency ~50-500 kHz) makes them a suitable candidate for hyperthermia applications [58-59].

***Size, Cellular Uptake Limit and Intoxicity*:** The core particle size of 37 nm and hydrodynamic particle size of 100 nm is found to be the limit for cellular uptake of polyvinylpyrrolidone (PVP)-coated iron oxide nanoparticles (PVP-IOs) nanoparticles [60]. The nanoparticles should have higher colloidal stability, biodegradability and non-toxicity in order to be administered as multimodal agents for biomedical applications in human [18].

The physical parameters of nanomaterials are heavily altered with the variation in their shape and size. These properties need to be studied and optimized for their successful application. In order to investigate these properties, a detailed knowledge of their origin, its fundamental theory and dependence of these properties on external and internal parameters is required. The preceding sections deal with the basic understanding of optical and magnetic properties in justified order followed by their modification with varying conditions.

1.4 Origin of optical study

In 1850s, Michael Faraday conducted first notable scientific study on optical characteristics of metal NP as colloidal suspensions and metallic films. The phenomenon of PL was identified by English physicist G.C. Stokes and the word luminescence was introduced by E. Wiedmann in 1888 into the literature. Another significant work was reported by Gaustav Mie in 1908 on extinction of light by metallic sphere described mathematically [61]. The optical behavior of metallic nanoparticles of

different shape and size integrated with another nanosystem is still a matter of investigation using various theoretical simulations and their experimental verification.

1.4.1 Fundamental Theory of Optical Behavior

The study of optical behavior characterizes the response of surface plasmon electrons in a material to incident electromagnetic radiation. When a material is exposed to an electromagnetic radiation, various types of phenomenon take place due to the interaction of incident radiation with surface electrons. For every material, the incident radiation undergoes partial transmission, partial reflection and partial absorption. The optical properties which define material responses to incident light are termed as transmissivity, reflectivity and absorptivity. The materials show surface plasmon resonance (SPR) arising due to the coherent oscillation of conduction electrons on metal surfaces excited by electromagnetic radiation [62]. These resonant frequencies can be modulated over a wide range by modifying the shape, size and structure of the nanoparticles.

One of the important processes due to radiation-surface atom interaction is luminescence which is further characterized as fluorescence and phosphorescence based on the average lifetime of the electrons in the excited state. The electrons in atoms absorb energy when radiated by light of appropriate wavelength and jump to a higher energy level. After certain time, which may vary from femtoseconds to years for few cases, the electrons relax back to their original ground state, giving off the energy previously absorbed via one-step or multi-step relaxation in form of radiative or non-radiative recombination, as per the property of the system under investigation [63].

1.4.2 Optical Behavior of Electron Rich Elements (Gold and Silver)

The noble metals such as silver and gold are considered as exquisite scatterers and absorbers of visible light [64]. In addition, they possess the optical characteristics

essential for the multimodality. The different optical characteristics of these metals have been discussed in the following section.

(a) Surface Plasmon Resonance (Absorption Spectra)

Since the noble metals (Au and Ag) are the best choices due to their excellent and sharp SPR responses, several theoretical and experimental investigations have been carried out to study the optical absorption and scattering efficiency of these metals [65-66]. Gustav Mie derived the absorption efficiencies, known as Mie theory, for homogeneous metal spheres [61,67]. Based on the reported literature, which investigated the plasmon-resonant materials both experimentally and theoretically, the optical absorption or SPR peak for gold and silver nanomaterials were found to lie in the visible region of the electromagnetic spectra with remarkable intensities [68-70]. The positions of these peaks were found to be optically tunable by variation in shape and size of the corresponding nanoparticles. Lee and El-Sayed had published UV-Vis absorption spectra obtained from gold NPs of size ranging from 9 to 99 nm that shows resonances between 520-580 nm [8]. The silver nanoparticles of the size range 29 nm to 136 nm were found to show a resonance peak in between 418 nm to 425 nm as shown by Evanoff and Chumanov [71]. Besides the absorption properties, the emission peak of a material is also a decisive factor in its biomedical applications which has been discussed in the next section.

(b) Excitation and Emission Spectra

The study of fundamental laws of absorption and emission of radiation from matter is known as luminescence. It involves the emission of light by a substance on absorbing radiation of various energies sometimes accompanied by non-radiative recombination of electrons (Figure 1.2). The wavelength of emitted radiation is a characteristic of the luminescent substance instead of the incident radiation. In this case, an electron absorbs

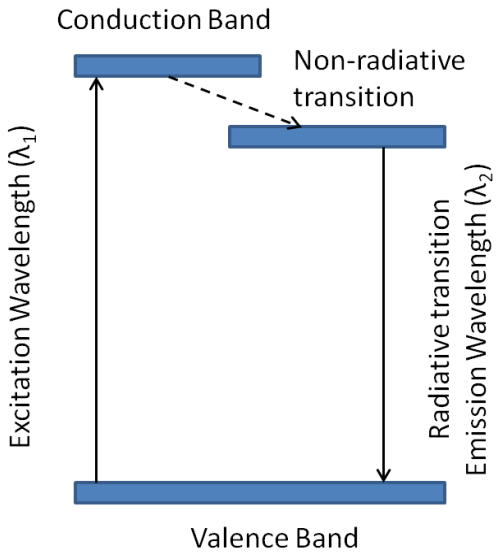

Figure 1.2 Photoluminescence principle indicating radiative and non-radiative recombination.

a light of wavelength λ_1, decays to lower energy state of excited electronic levels via non-radiative transitions. It then relaxes back to ground electronic state by emitting a light of wavelength λ_2 during radiative recombination. Since some energy is lost in this process, the wavelength λ_2 is larger than λ, ($E \propto \frac{1}{\lambda}$), however in resonance emission condition $\lambda_1 = \lambda_2$ [72].

The materials which are capable of emitting light most preferably in visible range are known as 'luminescent materials'. The efficient materials which can be put in to practical applications are those which can be easily produced in laboratory condition and has some degree of reliability and repeatability in their performance. The nanoparticles of noble metallic elements such as gold and silver are found to be fit in this criteria [73].

1.4.3 Effect of Optically Active Shell Material Coating on Dielectric Core

A wide study on effect of integration of gold and silver with dielectric cores such as silica, hematite, polystyrene and ZnS has been carried out from both theoretical and experimental point of view. It was then realized that optical properties of these core-shell nanostructures are tunable to a much wider extent in visible and near IR as compared to bare noble metal nanoparticles. P.K. Jain and co-workers, using Mie theory, calculated extinction wavelength maximum (λ_{max}) for different core-to-shell ratio in case of silica-gold nanoshells. They reported that values of λ_{max} can be tuned from 704 nm to 1160 nm by varying core size and shell thickness. The core sizes between 80 to 240 nm and shell thickness 10 nm to 35 nm were taken into consideration [67]. Xu and Hou synthesized Ag and Au coated magnetite nanoparticles with shell thickness varying from 0.5 to 2.5 nm on 10 nm core and measured absorption spectra for the obtained nanostructure. The SPR peak is found to lie in range of 500 to 600 nm [74].

In order to enhance the luminescence efficiency of weak luminescent materials, localized SPR absorption of coupled metallic nanoparticles is considered to be the most efficient method. The size dependence of PL spectra of silver and gold nanoparticles are attached with weak luminescent nanoparticles is of greater importance. Lin and group prepared germane-silicate fibers with gold nanoparticles embedded as cores and reported their visible to infrared luminescence along with enhanced quantum efficiencies [75]. They found a broad band in visible range and narrow band infrared PL from the synthesized microfibers with weak intensities. Sadat et al performed PL measurements for different sized Fe_3O_4 nanoparticle systems, poly (acrylic acid) (PAA)/Fe_3O_4, polystyrene spheres (PS)/Fe_3O_4 and silica coated PS/Fe_3O_4. For an

excitation energy of 3.04 eV the characteristic emission spectra shows broad peaks in scan range 465 to 900 nm with major peak centered near 560 nm while two less intense peaks near 690 and 840 nm [76]. Nanoparticles provide higher surface to volume ratio which also results in higher defect densities at surfaces. These surface defects are responsible for broadening of the emission peaks which further lowers their intensity [76]. The noble metal nanoparticles such as gold and silver can efficiently enhance the luminescence of a weak luminescent material up to many times, if there is a spectral overlap of surface plasmon absorption peak of the noble metal with absorption peak or emission peak of the other material. The overlapping of SPR absorption peak of silver as reported by D. Sarkar with the highest luminescence peak makes it a suitable luminescence enhancer for magnetite nanoparticles [47].

The magnetic behavior of the nanoparticles is the second property to be explored for their application as multimodal imaging agent. We will now describe the essentials of magnetism in the following section.

1.5 Magnetism

The study of magnetism in the early era of quantum mechanics revealed its origin from electron spins as well as exchange interactions. In recent days, the deeper understanding of magnetic properties allows us to use the magnets in day to day life in form of advance devices. The emerging area, where magnetic behavior of functional materials being explored is biomedicine.

1.5.1 Origin and Basic Theory of Magnetism

The origin of magnetism lies in the behavior of electrons in atoms. There are two types magnetic moment that contribute independently to the overall magnetism of a material - orbital magnetic moment and intrinsic spin moment of electrons. Thus, all atoms with a minimum of one electron show some sort of magnetism, even though, the useful

magnetic behavior is observable only in molecules and atoms consisting of unpaired electrons. This is due to Pauli's Exclusion principle which states that an orbital can have a maximum of only two electrons with anti-parallel spins, which effectively cancel magnetic moment of one another [77]. The transition metals such as cobalt, nickel and iron which possess unpaired d-electrons are most common examples of magnetic materials where spontaneous magnetization is observed. The magnetic behavior of these elements arises mainly due to exchange interaction between the electrons. The rare earth elements due to unpaired f-electrons including elements like Neodymium, Europium, samarium and cerium also exhibit magnetic properties. In the rare earth metals, the contribution of both spin and orbital motion is significant for their magnetic characteristics. In addition to these elements, many compounds, metal oxide and alloys of transition metals with rare earth metals also show strong magnetic properties [77-79]. Few materials exhibit strong response to the applied magnetic field and show a non-zero value of magnetization even in the absence of externally applied magnetic field afterwards. This type of materials such as Fe, Co and Ni are classified as ferromagnetic materials. The forces like direct exchange, superexchange, dipolar interactions as well as anisotropic forces are the key concepts involved in the study of these materials [51,77,80-81].

Direct Exchange: This exchange energy between two neighboring spins in a system via Heisenberg exchange interaction is given as [80-81]

$$E_{ex} = -2\sum_j J_{ij} S_i S_j \qquad (1.1)$$

Where J denotes the exchange coupling constant between two neighboring electrons i and j with S_i and S_j as their spin angular momentum vector, respectively. This interaction arises due to the electrostatic interactions that tend to align the spins in same direction. The alignment of spins depends on the sign of exchange constant. This force

is short-range and decays exponentially with the increase in distance between the neighboring spins.

Dipolar Interactions: The interaction energy between two magnetic dipoles is formulate can be given as [81-82]

$$U = \frac{1}{r^3}\left(\vec{\mu}_1.\vec{\mu}_2 - 3(\vec{\mu}_1.\vec{r})(\vec{\mu}_2.\vec{r})\right) \approx 10^{-4}eV \quad (1.2)$$

The dipolar interaction is very weak in nature and effective at low temperatures or in a system where the value of magnetic moment is high.

Anisotropic Energy: The anisotropy is defined as the dependence of an energy level of a particular direction. If the magnetic moments present in the materials are biased towards a unique direction [51], often termed as easy axis, the material is known to have uniaxial anisotropy [83]. The cubic materials such as iron and nickel have multiple easy axes and said to possess cubic anisotropy [77,84,85]. The crystalline structure of the material decides the type of anisotropy.

The spin orbit coupling in transition metals is responsible for anisotropic energy [86]. The fourth order approximation for uniaxial anisotropy ε_{uni}^{i} with magnetic moment $\mu_i$is expressed in form of energy density can be written as

$$\varepsilon_{uni}^{i} = -K_1\, cos^2\theta_i - K_2\, cos^4\theta_i$$
$$= K_1 S_z^2 + K_2 S_z^4 \quad (1.3)$$

Where $K_1$and K_2 denote the primary and secondary anisotropy constant, respectively, for the materials [85]. These constants are generally obtained using experimental techniques and expressed as temperature dependent energy-density. Here θ_i is the angle between the easy axis and S_i.

In case of cubic anisotropy, the parameterization can be done as

$$\varepsilon_{uni}^{i} = K_1\left(S_x^2S_y^2 + S_y^2S_z^2 + S_z^2S_x^2\right) + K_2\left(S_x^2S_y^2S_z^2\right) \quad (1.4)$$

The positive value of K_1 yields the easy axes of a crystal system along body edges (100) whereas a negative sign generates the easy axes along body diagonals (111) [77,85].

For magnetite (Fe_3O_4) cubic crystals, at T = 300 K [85] [39];

$$K_1 = -1.35 \times 10^5 ergs/cm^3$$

$$K_2 = -0.44 \times 10^5 ergs/cm^3$$

Mean Field Approach: The average exchange interactions, many a times, are treated as effective magnetic field in a theory called mean field approximation. The Weiss theory or the mean field theory was developed in order to account for these type of interactions. They postulated the occurrence of an additional magnetic field (H_W) with a non-magnetic origin. This field was termed as molecular field and added to the external field [87], making the equation

$$M = M_S \mathcal{L}\left(\frac{\mu_0 m_0 (H_a + H_W)}{kT}\right)$$

$$= M_S \mathcal{L}\left(\frac{\mu_0 m_0 (H_a + N_W M)}{kT}\right) \quad (1.5)$$

where N_W is the characteristic of the materials.

For higher temperatures, one finds the famous Curie-Weiss law that states the dependence of susceptibility on temperature as

$$\chi \propto \frac{1}{T - T_C}, \quad (1.6)$$

where

$$T_C = \frac{\mu_0 m_0 M_S N_W}{3k} \quad (1.7)$$

In this equation, T_C is the characteristic of every material termed as Curie temperature. For temperature greater than T_C, the paramagnetic behavior is observable in the materials [77,88]. The Weiss theory states about the magnitude of magnetization whereas no information about its direction is provided [87]. This drawback has been

overcome by the use of micromagnetics which can predict the magnetization direction at each location inside the magnetic system.

1.6 Domain Formation and Superparamagnetism

In 1907, P.E. Weiss, in an attempt to explain ferromagnetism proposed domain theory. According to the theory, actual specimens of ferromagnetic solid comprises of a large number of small regions called domains, each of which are spontaneously magnetized up to saturation extent (Figure 1.3) [77]. The magnetization direction for different domains is randomly oriented. The size of these domains varies from 1- 100 μm which are separated from each other by a domain wall. The ferromagnetic and ferrimagnetic materials show single domain, multidomain and superparamagnetic properties depending upon their particle size. The reason for formation of domain is the minimization of total energy that also includes magnetic anisotropy, the exchange as well as magnetostatic energies. The reason behind formation of domain walls, also known as Bloch walls, is the energy associated with the distribution of surface moments, often termed as magnetostatic energy.

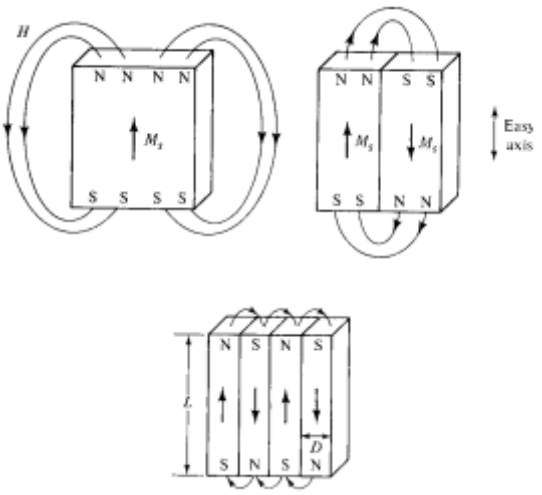

Figure 1.3 Division of crystal into domains [77].

For a large single crystal, considering a uniformly magnetized single domain, the surface magnetic moments form at the ends, due to the magnetization which also act as second source of magnetic field. The magnetostatic energy associated with surface charge distribution reduces to half, if the magnetization splits into two domains which are magnetized in opposite directions in turn decreases the spatial extent of demagnetizing field [77]. This subdivision of domain is not indefinite as formation of domain walls require energy which needs to be preserved. The interfaces between the regions with different magnetization directions are called domain walls that have finite width determined majorly by magnetocrystalline and exchange energy. The exchange energy keeps the spin parallel and is major decisive factor in domain wall thickness,

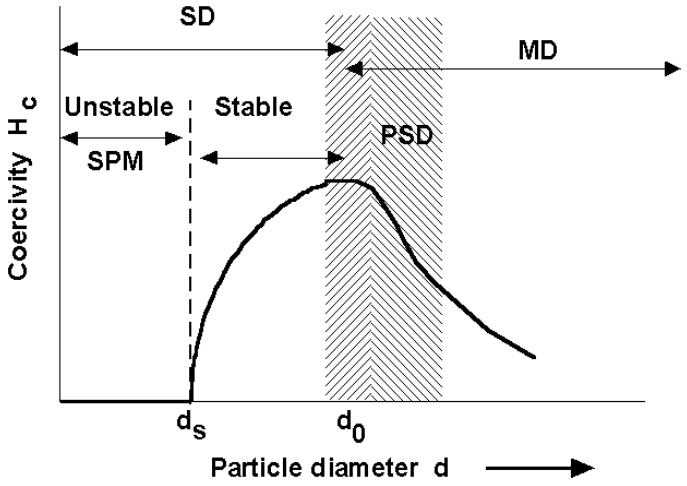

Figure 1.4 Types of Domains in different particle size range of the nanoparticles [90].

smaller value and larger value leading to wider and thin walls, respectively. The anisotropy energy, on the other hand, tends to make the wall thinner as possible. These counter effects leads to the formation of domain walls of limited width (~100 nm) and surface energy. The magnetic properties such as coercivity and remanence hint the existence of magnetic domains which has strong correlations with grain size [89].

The magnetic behavior can be classified depending on the grain size in four ranges as

shown in Figure 1.4. Multidomain, Single-domain, Pseudo-domain and Superparamagnetic [90].

1.6.1 Multidomain

A bulk magnetic body consists of a number of sub-magnetic domains, forming a multidomain structure. According to Weiss, in absence of an applied field, the magnetic moments corresponding to each domain aligns only within the magnetic domain. The alignment direction for magnetic moments of domains is independent of the neighboring domains. On application of an external magnetic field, the magnetic moments of individual domains align themselves towards applied field direction.

The experimental evidence suggests that magnetic moments alignment occurs possibly due to domain wall motion instead of simple alignment of moments. The domain walls shift in favor of domains having magnetic moments aligned parallel to the applied fields. This domain wall motion is generally found to be jerky and discovered in 1919 known as Barkhausen effect [77].

1.6.2 Single - Domain

A sufficiently small magnetic material can reach a single domain state where it will not contain domain walls. If the total magnetostatic energy for a single domain particle of size d, which is proportional to particle volume d^3, whereas the domain wall energy and area varies with cross- sectional area of the particle d^2. If only these energies are taken into account, a critical diameter d_c exists below which the single domain magnetic state is favored. The critical size for single- domain state is dependent on the magnetostatic energy and domain wall energy for a material. Using this formulation, the solution usually ends up as a function of domain wall energy and saturation magnetization (M_s) stated as [78]:

$$d_c \approx \frac{18\sqrt{A_{ex}K}}{\mu_0 M_s^2} \quad (1.8)$$

Where A_{ex} is the stiffness constant and μ_0 is the permeability for free space. The critical size for single domain is nearly equal to the domain wall thickness and is expected to be formed with the less than 1000 atoms in diameter. The typical values for d_c are about 15 nm, 35 nm, 100 nm & 750 nm for Fe, Co, NdFeB and $SmCo_5$ respectively.

A single domain grain is uniformly magnetized to a value of its saturation magnetization. The transition from multidomain to single domain state is accompanied with a high increase in the coercive field ($H_c \cong \frac{K}{3M_s}$, for uniaxial symmetry) [91].

1.6.3 Pseudo Single Domain

The experiments showed that there is no sudden transition between single domain and multi domain state, but a smooth change which covers a relatively larger range of grain size. The magnetic behavior in this transition region has single domain (high remanence) like as well as multi-domain (low coercivity) like aspects known as Pseudo single domain as called by Stacey (1962). This behavior is observed for the size range between 100 nm - 20 μm depending on the material [77].

A lot of theoretical and experimental works have been carried out on pseudo-single domain grains. The most convincing theory related to multidomain particles suggests that small multidomain particles which contain less number of domains can actually resist nucleation of domains. In few cases, the multidomain grains exist in metastable single domain state. The change from one domain state to other domain state is called transdomain transformation.

1.6.4 Superparamagnetism

For a single domain particle, the anisotropy energy in first approximate is directly proportional to the volume of particle. In case of uniaxial anisotropy, the energy barrier associated with the separation of easy magnetization directions is E_b= KV, where K is the anisotropy energy constant and V is the volume of particle [51,81,87]. The

anisotropy energy decreases with decreasing particle size and below a characteristic size the value of KV becomes comparable or lower than the thermal energy k_bT which means the energy barrier can be overcome leading to thermal fluctuations of the spin magnetic moment across easy axes, similar to the case of single spin for paramagnetic system. In this way, the whole spin system may be rotated while retaining the ferro- or antiferromagnetic coupling of the spins inside that single domain magnetic system [81]. The behavior of a magnetic material like a paramagnet under low-field conditions and ferro-ferrimagnetic under externally applied high magnetic field is called Superparamagnetism. This behavior is exhibited by particles within a particular size range [85]. In order to decide the superparamagnetic behavior of a magnetic material, different anisotropies play a significant role as summarized below.

1.7 Magnetic Anisotropy

For a uniaxial single domain particle, the magnetic anisotropic energy is given by $(\theta) = KV\ sin^2\theta$, where V denotes the particle volume and θ is the angle between applied field and magnetization axes [77]. Depending upon different origin source, they are classified as:

(a) ***Magnetocrystalline Anisotropy***- This kind of anisotropy arises from the spin-orbit coupling. It is responsible for strong coupling between the electron spin with orbital state of electron and thus the crystal lattice. Due to its strong correlations with crystal structure, it is highly dependent upon the symmetry considerations of the system [77].

(b) ***Shape Anisotropy***- The magnetic anisotropy that results from shape of the specimen is termed as shape anisotropy. A monodomains spherical particle which is uniformly magnetized has no shape anisotropy since the demagnetizing factors in all directions are isotropic. In case of non-spherical particles, the samples easily magnetize along longer axis as compared to shorter ones. This is possibly due to smaller values of

demagnetizing filed along longer direction which arises because of larger distances between the induced dipoles at the surface sample [77,81].

(c) ***Strain Anisotropy***- Strain anisotropy is the secondary effect related to strains at the sample surface. It is generally a magnetostrictive effect and due to the magnetostriction, the strains are prevalent in the direction of magnetization [81].

(d) ***Surface Anisotropy***- The presence of large number of surface atoms at the nanoparticle surface gives a sufficient amount of anisotropy contribution termed as surface anisotropy [77].

(e) ***Exchange Anisotropy***- The exchange interactions between the two atoms at the interface composed of two materials give rise to significant amount of exchange anisotropy which is clearly observed as exchange bias effect. This exchange bias depends upon the type of magnetic property shown by the two distinct materials at the interface [81].

1.8 Characteristics of Superparamagnetic Materials

The superparamagnetic materials exhibit most of the key magnetic properties that are an essential requirement in various biomedical detection modalities. The utilization of magnetic nanoparticles in these applications is generally proportional to their magnetic moments because higher moment values result in greater force and much better detection signals [28,42,81].

1.8.1 DC Magnetization Measurements

Temperature dependent magnetization studies:

The zero-field-cooled (ZFC) and field-cooled (FC) magnetization curves are the most common ways to characterize the magnetic nanoparticles. A typical ZFC and FC curve for a magnetic material is shown in Figure 1.5 [92]. For ZFC magnetic measurement, the samples are first cooled in absence of magnetic field. The magnetization data is then

recorded during heating after application of constant magnetic field with respect to temperature. In order to obtain FC magnetization data, the same protocol is applied as that of ZFC with the only exception that cooling is done in presence of a small applied field. The curves tend to provide the magnetism history of materials under observation [93].

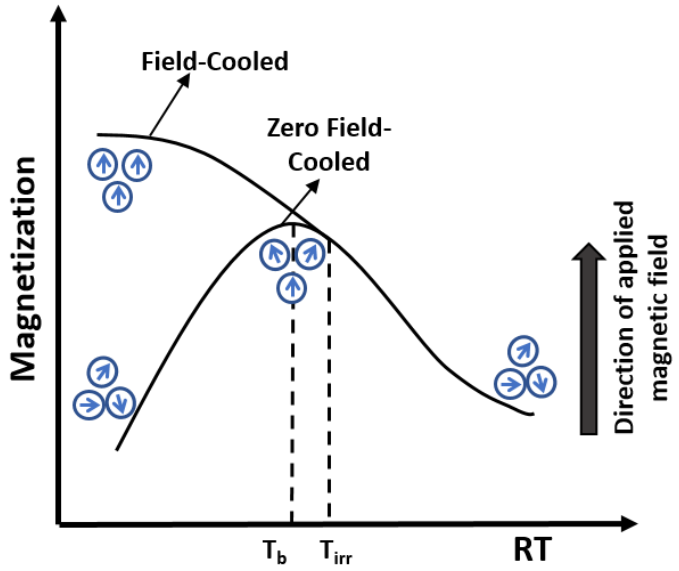

Figure 1.5 ZFC and FC variation of magnetization with temperature.

When the material is cooled in absence of any magnetic field, their magnetic moments are assumed to be frozen in random directions at lower temperature below the complete blocking process. On an application of small magnetic field, there are changes in the magnetization directions. The value of magnetization, for monodomains with uniaxial symmetry, at lower temperatures below the blocking temperature was first reported by Gittleman in 1974 as $M_{ZFC} = \frac{H_{eff}M_{nr}^2}{3K}$; where M_{nr}, K and H_{eff} signifies the non-relaxing magnetization (the averaged magnetization along core spin direction), anisotropy constant and effective magnetic field, respectively. After a maximum value

of magnetization is achieved at a particular temperature, M_{ZFC} achieves a thermodynamic equilibrium state. At the temperature higher than blocking temperatures, the value of M_{ZFC} can be written as $M_{ZFC} = M_{nr}\mathcal{L}\left[\frac{M_{nr}VH_{eff}}{kT}\right]$. Using low field approximation for Langevin function: $\mathcal{L}(x) \approx {}^{x}/_{3}$, the magnetization value reduces to $M_{ZFC} = \frac{M_{nr}^2 V}{3kT} H_{eff}$. These equations are valid for non-interacting particles [85,92,94]. For monodispersed nanoparticles, a maximum peak in ZFC curve at blocking temperature is observed. In case of real systems, there is a distribution of particle size which results in a slightly higher blocking temperature and the curve maxima corresponds to blocking temperature for the largest particle in the system [85].

The experimental studies have demonstrated a strong dependence of ZFC and FC magnetization curves on the interparticle interactions. For the field-cooled measurements, since an appreciable number of large particles are blocked at initial temperature, a preferred orientation of magnetic moments is retained below the blocking temperature. The magnetic states for blocked particles are highly dependent upon thermal history of samples which alters the M_{FC} value. This is the main reason behind smaller values of magnetic moments in case of ZFC as compared to the FC values [85,94]. The ZFC and FC curves coincide with each other above the bifurcation temperature indicating ergodic behavior of the system at higher temperature which is independent of the applied cooling field. With increase in the strength of interparticle interactions, the peak maximum is observed to shift at higher temperatures. For weakly interacting particles, the magnetization value increases with decrease in temperature is much pronounced due to blocking of magnetic moments corresponding to smaller particles [81,85]. However, in case of strongly interacting system, the magnetization value remains almost constant even below the blocking temperature. This behavior of materials leads to the formation of a collective state where dipole interactions come into

play leading to transformation in a spin-glass like state [81,94,95]. The blocking temperature of the nanoparticle system is also helpful in determining the effective anisotropy constant (K_{eff}) for the system under study. The Stoner- Wohlfarth expression provides the relationship between two as: $< T_B > = \frac{K_{eff} * V}{25 * k_B}$. The variation in K_{eff} for different nanoparticle systems is related to the simultaneous effect of interparticle interactions and surface anisotropy [82,95]. The nanoparticles tend to have higher values of anisotropy constant due to prominent surface effects.

Field Dependent Magnetization Studies:

The field dependent magnetization studies for a particle at a given temperature determine its magnetic behavior and gives information about the saturation magnetization, coercive field and remnant magnetization (Figure 1.6) which are the key deciding factors for their application [96].

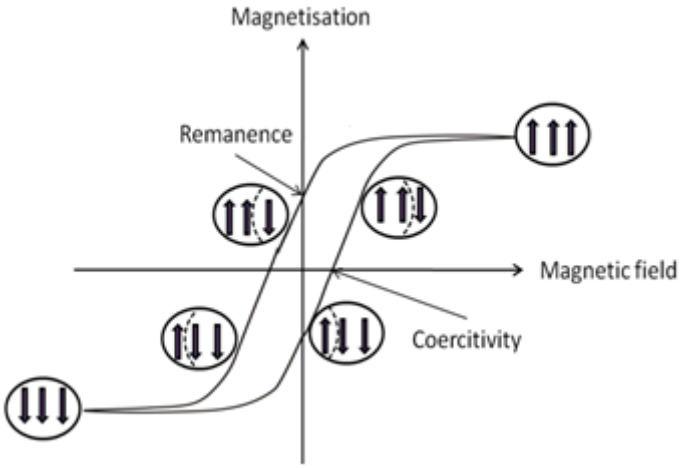

Figure 1.6 Variation of magnetization with applied field depicting coercive field and remanence magnetization [96].

Saturation Magnetization:

For a magnetic material that consists of n number of atomic magnetic dipoles with magnetic moment m per unit volume, the saturation magnetization M_s is calculated to

be equal to $M_s = n \times m$. This M_s value is unique property for each material which sets a maximum magnetization achievable for a specific magnetic material [77]. The elements Fe, Ni and Co are most widely used materials due to their high M_s values and ease in synthesis as nanoparticles [82,98]. This value of saturation magnetization enhances with the increase in particle size due to reduction in surface effects such as spin canting. The M_s values of magnetic nanoparticles are way smaller than the bulk materials due to hindrance provided by surface energy in perfect alignment of spins along a single direction on application of an external magnetic field. The saturation magnetization for spherical nanoparticles can be estimated as: $M_{np} = M_s(bulk)[(r - \Delta)/r]^3$, where r and Δ denote particle radius and thickness of magnetically frustrated layer at the surface, respectively [95]. The reduction in surface effect is possible by modification of particle shape. A magnetically dead layer on surface appears due to decrease in coordination as well as absence of oxygen causing reduction of M_s value when compared to that of bulk sample in Fe_3O_4. The thickness of magnetically dead layer (t) can be calculated using the formula [97]:

$$M_s = M_s(bulk)\left(1 - \frac{6t}{D_{TEM}}\right) \quad (1.9)$$

Where D_{TEM} denotes the particle size of nanoparticles obtained using characterization techniques like transmission electron microscopy (TEM) and $M_s(bulk)$ is the saturation magnetization of the particles in bulk state.

Coercive Field:

The coercivity of magnetic materials plays an important role in their consideration for an application, as it provides idea about the magnetizing field required to reverse the magnetization direction [77]. At lower temperatures where the maximum spins are blocked to a particular direction, the value of coercive field (H_C) is same as the one expected for single domain magnetic structure. In particles with uniaxial symmetry

$H_C = H_{C0} = \left(\frac{1}{2}\right) H_k$. Here $H_k = \frac{2K}{M_{nr}}$, where K denotes the overall anisotropy constant and M_{nr} represents non-relaxing magnetization [85]. At higher temperatures, the relaxation time for fluctuations of magnetic moments is much smaller than the measuring time. This results in zero coercivity value at higher temperatures which is one of the important signatures of superparamagnetism in magnetic materials. At the intermediate temperatures, the value of H_C can be formulated as:

$$H_c = H_{c0}\left[\left(1 - \sqrt{(T/T_B)}\right)\right] \quad (1.10)$$

where T_B is the blocking temperature of the corresponding particles and H_{c0} is coercive field for monodomains [85].

For negligible magnetic anisotropy, the magnetization of superparamagnetic nanoparticles is proportional to the externally applied magnetic field (H) and temperature, which is expressed as Langevin function [51]:

$$M\,(H) = M_s^{spm} L\left(\frac{\mu H}{k_B T}\right) \quad (1.11)$$

At low externally applied magnetic fields, the nanoparticles show a linear increase in magnetization values. The significance of disordered magnetic spin layer can be realized on splitting the paramagnetic and superparamagnetic contributions to the value of magnetization by fitting the M-H data of samples at room temperature by addition of a linear term. The modified Langevin equation can be formulated as [98]:

$$M\,(H) = M_s^{spm} L\left(\frac{\mu H}{k_B T}\right) + PH \quad (1.12)$$

Where M_S^{spm} denotes M_s value of superparamagnetic part, μ is the average magnetic moment associated with uncompensated spins of the nanoparticles and P is the paramagnetic contribution to the susceptibility varying with field.

Remanence Magnetization:

The residual magnetism left in a magnetic material on removal of the applied magnetic field gives remanent magnetization. On application of a dc magnetic field, three different types of remanent magnetization curves can be obtained namely- thermoremanent magnetization (TRM), isothermal remanent magnetization (IRM) and demagnetization (DcD) curves [85]. The measurement protocols to obtain these magnetization curves are as follows:

(a) **TRM**: The field is applied at temperature well above the average blocking temperature. The sample is then cooled to a fixed temperature of interest and the magnetization is measured after removal of the externally applied field.

(b) **IRM**: The sample is cooled to the lower temperature, which is the measurement temperature, from a higher temperature in absence of any magnetic field. On reaching the measuring temperature, an external field is applied and removed subsequently. The magnetic field is applied to the material only when it has achieved thermodynamic equilibrium.

(c) **DcD**: In this type of magnetization study, the sample is first cooled to the desired lower temperature in zero field condition. The material is then saturated to the remanence IRM = IRM (H = ∞), and a field in the opposite direction is applied which is subsequently removed.

The time decay measurement of remanence magnetization is one of the tools used to study the magnetization dynamics and reversal mechanisms.

1.8.2 AC Susceptibility Measurements

When an alternating magnetic field $H(t) = H_0 \sin(\omega\tau)$ is applied, the magnetization $M(\omega) = \chi_{ac}(\omega, \tau)H_0$ for the magnetic nanoparticles is recorded. The nanoparticles tend to exhibit a delayed magnetic response due to finite rate of changes in magnetization.

This property is modeled using two components comprising of in-phase (χ') and out-phase (χ") component with respect to ac field expressed as: $\chi_{ac}(\omega,\tau) = \chi'(\omega,\tau) + \chi''(\omega,\tau)$. For a particle system that shows dc magnetic susceptibility $\chi_{dc} = {}^{M}/_{H}$ and τ as effective relaxation time, the χ' and χ" has been formulated as

$$\chi' = \frac{\chi_{dc}}{1+(\omega\tau)^2} \tag{1.13}$$

and

$$\chi'' = \frac{\chi_{dc}\omega\tau}{1+(\omega\tau)^2} \tag{1.14}$$

The measurement of ac magnetic susceptibilities for a range of frequencies is another important investigation tool to study the magnetization dynamics of the system, as they have a larger window of measurement time with the same technique [85].

Several models were proposed to fit the ac magnetic susceptibility curves in order to gain information about spin dynamics of the system under investigation. Gittleman, in 1974, proposed an equation for magnetic susceptibility for an assembly of non-interacting polydispersed single domain particles with randomly oriented easy axes. It does not account for the oscillations of magnetic moment in the anisotropy energy potential well, i.e, for transverse relaxation. Later, Khater et al. in 1987 performed the calculations for ac magnetic susceptibility using Poisson volume distribution which is also similar to Gittleman approach that used non-realistic volume distribution function [51,81,85]. In case of small magnetic nanoparticles, the interparticle interactions play a significant role in the dynamics of spin which allows the moments to interact with each other that may lead to long-range or short-range order. The different types of important interactions are as follows:

***Dipole-dipole Interaction*:** This is a long-range anisotropic interaction which depends upon the separation between two magnetic dipoles, say, m_1 and m_2, separated by a distance r. The dipolar interaction energy for the pair of particles can be written as [99]:

$E_{d-d} = \frac{m_1.m_2}{r^3}$. If the outermost layer is non-magnetic which causes physical separation between the two magnetic particles, the dipolar interaction energy reduces according to the relation [82]:

$$\frac{E_{d-d}(\alpha)}{E_{d-d}(0)} \sim \frac{d_{Tem}^3}{(d_{Tem}+\alpha)^3} \quad (1.15)$$

In this formula, α and d_{Tem} represents the magnetic core-to-core spacing and mean nanoparticle size obtained from TEM micrographs, respectively.

***Direct Exchange Interaction*:** This kind of interaction is caused due to quantum mechanical effect which leads to long range magnetic ordering [77,93]. If the exchange interaction takes place between neighboring magnetic atoms, it is called direct exchange. It plays a significant role when the surfaces of the particles are in close contact with each other.

***RKKY Interaction*:** This specific type of interaction takes place when both the matrix and the particles are metallic in nature. It is inversely proportional to the cube of interparticle distances [94].

***Superexchange Interaction*:** As discussed, direct exchange requires hopping between the orbitals which are typically localized d-orbitals for transition metals. In most of the case of transition metal oxides, large intermediate oxygen anions are present between the transition metal cations. In these cases, the direct hopping of electrons between the d-orbitals is very unlikely. So, the concept of direct exchange for such cases can be taken in account by considering hopping via intermediate p-orbital. This type of interaction is termed as superexchange interaction [77,85,100].

An order parameter Ø that can quantify the relaxation characteristics of the system can be obtained using the maxima temperature values of ac magnetic susceptibility for a particular frequency. It is defined as [101]: $\emptyset = \frac{\Delta T_{max}}{T_{max}(f)\Delta \log(f)}$. The value of Ø gives a

hint about the magnetic behavior of the ensemble on an average and is categorized as follows [102]:

(i) $\emptyset \sim 0.3$ (for superparamagnets)

(ii) $\emptyset \sim 0.10 - 0.13$ (for non-interacting nanoparticles)

(iii) $\emptyset \sim 0.05 - 0.13$ (for interacting nanoparticles)

(iv) $\emptyset < 0.005$ (for spin-glass systems)

The strength of interparticle interaction between the magnetic nanoparticles decides the magnetic behavior of the ensemble. The order of relaxation time τ characterizes and provides information about the behavior using the following expression [93,104,105]:

(i) Superparamagnetism, Neel-Arrhenius (NA) equation: $\tau = \tau_0 exp\left(\frac{-E_a}{k_B T_f}\right)$

(ii) Glass-like freezing, Vogel-Fulcher (VF) law: $\tau = \tau_0 exp\left(\frac{-E_a}{k_B(T_f - T_0)}\right)$

(iii) Superspin glass (SSG), Power law (PL) model: $\tau = \tau_0 \left[\frac{T - T_g}{T_g}\right]^{-zv}$

The Néel Arrhenius (NA) formalism is used for the ensembles with individual and independent magnetic behavior without taking into account any interparticle strength. For superparamagnetic nanoparticles, the value of τ_0 is of the order of 10^{-13}-10^{-15} s [106]. With increase in strength of interparticle interaction, a collective behavior is encountered. The NA equation is modified by the addition of a new term called 'glass temperature (T_g)' in the denominator. This modified equation is termed as Vogel-Fulcher law. The τ_0 value for cluster spin-glass lies in the range 10^{-6}-10^{-10} s for cluster-glass behavior [107]. For much greater interparticle interactions, a superspin glass phase with higher spatial randomness and magnetic frustration is observed. The Power law model fit for magnetic spin relaxation time characterizes this particular type of phase with a critical exponent zv whose range normally lies in between 4-13 for systems with superspin glass behavior. The parameter ν relates correlation length ξ with the glass

temperature as $\xi \propto \left(\frac{T_p}{T_g} - 1\right)^{-v}$. The value of τ_0 is obtained to be in the range of 10^{-11}-10^{-13} s for spin-glass systems [108].

1.9 Magnetic Relaxation in Nanoparticles

We consider a system consisting of N particles possessing a uniaxial symmetry. The anisotropy energy in usual axis system, for a particle of volume V in absence of an external field is given as $E=KV \sin^2\theta$, where K denotes the anisotropy constant.

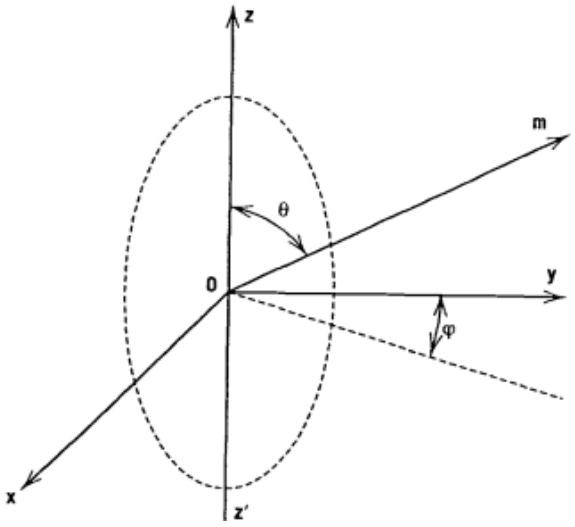

Figure 1.7 Spherical coordinate system. The magnetization easy axes is along ZOZ′ [85].

For positive K values, OZ and OZ′ are the easy axes with same value of energy minima (Figure 1.7) [85]. Thus, at thermodynamic equilibrium the two energy minima are equally populated. If at a given time t, P is the number of particles with magnetic moment m pointing towards OZ, then N-P particles points towards OZ′ easy axis. After time dt the particles with m pointing towards OZ and OZ′ gets modified and the change is written as

$$dP = \frac{(N-P)}{2\tau}dt - \frac{P}{2\tau}dt$$

Where, $\frac{1}{2\tau}$ denotes time unit probability for 'm' reversal. If M_{0r} is taken as non-relaxing magnetization with relaxation time τ and S_0 as initial value of $\frac{2P}{N-1}$, the magnetization towards OZ can be represented as

$$M = M_{0r}S_0 exp\left(-\frac{t}{\tau}\right) \tag{1.16}$$

On application of a field H along OZ axis, the energy can be written as $E = KV\ sin^2\theta - HM_{0r}Vcos\theta$. Thus, the two minima of the energy values are unequal which leads to existence of two probabilities: $1/\tau^+$ and $1/\tau^-$, for jump from lowest minima to upper minima and the opposite reversal, respectively. Therefore,

$$dP = \frac{(N-P)}{\tau^-}dt - \frac{P}{\tau^+}dt$$

and modified magnetization along OZ axis as $M = M_{0r}[S_1 + (S_0 - S_1)exp\left(-\frac{t}{\tau}\right)]$, where $S_1 = \frac{\tau^+ - \tau^-}{\tau^+ + \tau^-}$ and $\frac{1}{\tau} = \frac{1}{\tau^+} + \frac{1}{\tau^-}$. For thermodynamic equilibrium to be achieved, $t > > \tau$ or $S_0 = S_1$. So, in case of non-zero magnetization along H, few part of magnetization i.e. S_1 is blocked while the remaining $1 - S_1$ relaxes with relaxation time τ. So for $H = 0$, the time for direction change is 2τ while for a complete back and forth process, it is equal to 4τ [85].

1.10 Different Models of Relaxation

The magnetic spin system, on removal of applied magnetic field, relaxes to its minimum energy state in a very slow manner. A typical relaxation curve is obtained as depicted in Figure 1.8 [109]. In case of most of the models, an exponential relaxing behavior is observed given as [104]:

$$M(t) = M_0 exp\left(-\frac{t}{\tau}\right); \tag{1.17}$$

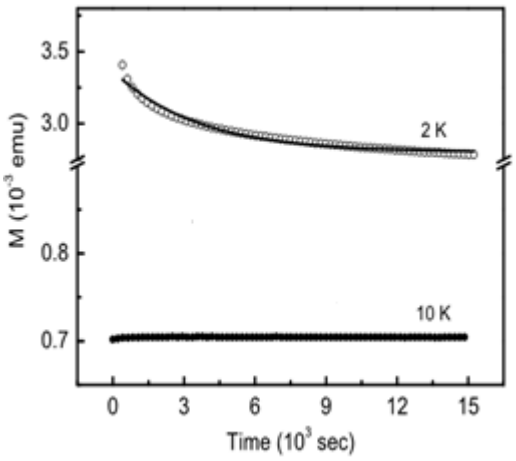

Figure 1.8 Magnetic relaxation measurement at 2 K and 10 K in presence of 2T applied magnetic field for CoPt nanoparticles indicating superparamagnetic relaxation. [109].

where τ is the time constant in an ideal case. For real system, there is a distribution of relaxation times due to a comparatively wide range of energy states which gives rise to a stretched exponential form of function stated as [105]:

$$M(t) = M_0 - M_r \exp\left[-\left(\frac{t}{\tau}\right)^{1-n}\right]; \tag{1.18}$$

which describes the relaxation behavior for spin glass.

Figure 1.9 shows relaxation curves for polycrystalline Ru-Copper oxides with spin-glass properties at 400 K for different waiting times [101]. The values M_0 and M_r corresponds to intrinsic ferromagnetic and spin-glass components of the observable relaxation effects with major contribution from M_r component. The M_r and τ values are dependent on temperature and waiting time whereas n is only temperature dependent parameter.

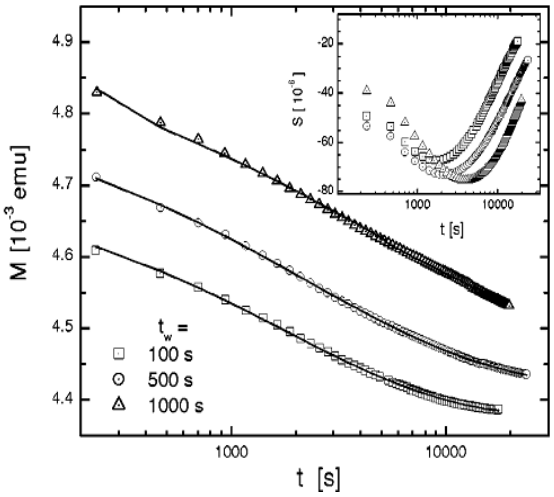

Figure 1.9 Relaxation curves of m^{TRM} vs t after FC in $\mu_0 H$ = 0.46 mT from T=400 K toT_m=294 K after different waiting times t_w for polycrystalline Ru-Copper oxide [101].

For a uniform distribution of energy barriers ranging from zero to some constant energy value, there is an observable logarithmic decay for magnetization value in accordance to equation [110]

$$M(t) = M_0(t)\left[1 - S(T)\ln\frac{t}{\tau}\right]; \tag{1.19}$$

with $S(T)$ representing the magnetic viscosity $\frac{1}{M_0}\ \frac{dM}{d\ (\ln t)}$.

For a critical slowing down process of magnetic relaxation time, the power law form $M(t) = M_0 t^{-n}$ is used to study the magnetization decay, where n is temperature dependent exponent [82]. The magnetic characterization of magnetite coated gold nanoparticles with average size of 14 nm has been reported by Felix et al [99]. The value of empirical parameter Ø calculated from χ' measurement (Figure 1.10) represented the weak interaction among the particles. For the nanoparticle system, the dipolar interaction is reported to be inversely proportional to the physical separation between the particles. The origin of exchange anisotropy for the system is the outcome of interaction between magnetically ordered layer of Fe_3O_4 shell and disordered spins of

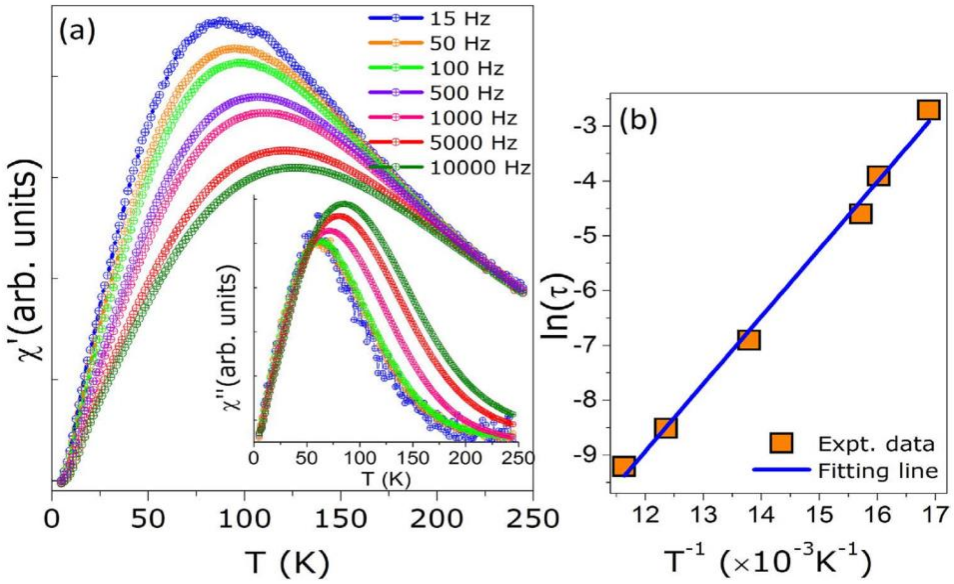

Figure 1.10 Temperature dependence of real part of magnetic ac susceptibility at different frequencies and out-of-phase component as inset (a); relaxation time as function of inverse of maximum temperature (b). The fitting line corresponds to Neel-Arrhenius fit [99].

gold core situated at the interface. A decreasing trend in exchange bias field is observed with increase in temperature.

The observation of more than one magnetic behavior is also possible in a single magnetic system. L. Shlyk et al studied the magnetic spin relaxation mechanism of kagome ferrite $SrSn_2Fe_4O_{11}$ [111]. From the data analysis of frequency dependent ac magnetization along with temperature dependent dc magnetization values, they reported the coexistence of ferromagnetic and spin-glass-like behavior for the system. For temperature greater than 20 K, the maximum temperature of ac susceptibility follows the Arrhenius law. Below T<20 K, deviation from Arrhenius and Vogel-Fulcher law was observed tending to the conclusion that a non-thermal relaxation is active in low-

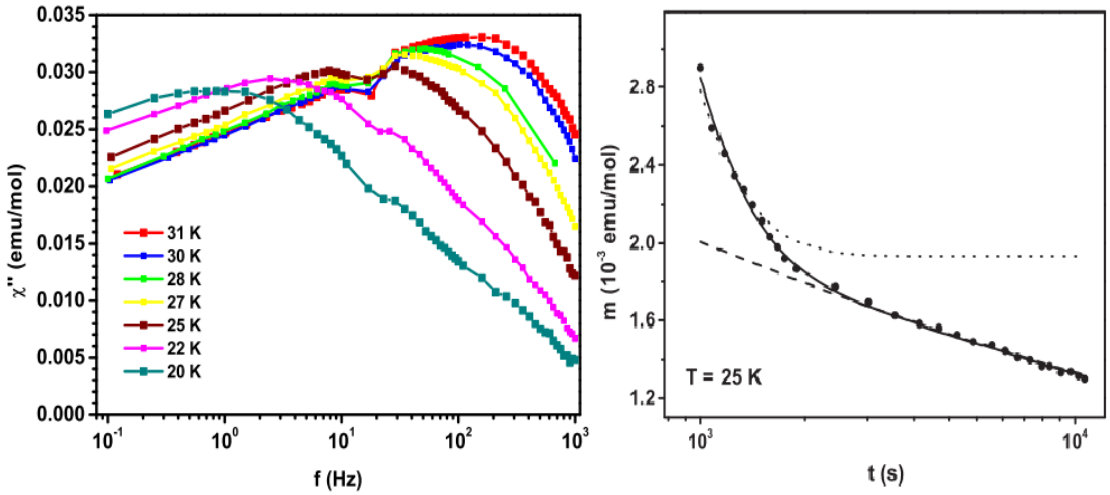

Figure 1.11 Frequency dependence of χ" at different temperatures and thermo-magnetic relaxation of $SrSn_2Fe_4O_{11}$ single crystal at T=25 K. The relaxation curve fit shows co-existence of two types of relaxation behavior for a single system [111].

temperature regime. The presence of double peak structure for χ″(f) points towards the existence of multiple relaxation processes. The thermomagnetic relaxation data fits shown in Figure 1.11 also emphasizes on the presence of two relaxation processes as the proper curve fit is obtained only after the superposition of power law and exponential forms for magnetic spins.

It can be summarized that the superparamagnetic iron oxide nanoparticles possess combination of most of the desirable properties such as superparamagnetism, high saturation magnetization values, stability and biocompatibility, imaging capabilities and flexible surface modification / conjugation which make them very efficient to be used in various biological applications. The integration of these SPIONs with electron rich metal i.e. silver makes them optically active and acts as luminescence enhancer for magnetite nanomaterials. However, there is no comprehensive study on the magnetic properties and its relaxation behavior of core-shell magnetic nanoparticles, in the size range suitable as a multimodal imaging agent. In order to do so it is essential to synthesize monodispersed bare magnetite and noble metal coated magnetite

nanoparticles of different shell thickness and study their structural, optical and magnetic properties which could be employed as multifunctional materials in biological imaging, drug delivery and hyperthermic treatment of cancerous tissues or tumors.

1.11 Thesis Aims

The specific objectives of the PhD thesis are as follows:

1. Theoretical investigation of the critical size range/ core-shell ratio of magnetite-silver nanoparticles as well as tuning of synthesis parameters to obtain uncoated and silver coated magnetite nanoparticles in the desirable size range (<40 nm) and their effect on particle morphology and size.

2. Effect of selected metal coating on magnetite nanoparticles on their optical characteristics.

3. Study of structural and magnetic properties of the synthesized core-shell magnetite nanoparticles.

4. Study of magnetic relaxation behavior of so obtained core-shell nanoparticles.

and

5. Possible use of these core-shell magnetite nanoparticles for therapeutic applications such as magnetic hyperthermia.